University of North Carolina Asheville
Journal of Undergraduate Research
Asheville, North Carolina
May 2018

In-vitro and *In-silico* Synthesis of Anticancer Compounds to Halt Rapid Cell Division and Cleave DNA

Malina L. R. Navarez
Chemistry
The University of North Carolina Asheville
One University Heights
Asheville, North Carolina 28804 USA

Faculty Advisors: Dr. Jalisa H. Ferguson, Dr. Herman L. Holt

Abstract

Combretastatin A-4, a naturally occurring compound isolated from the South African bush willow *Combretum Caffrum*, has derivatives such as chalcones. These compounds contain antibacterial, anti mitotic, anticancer, and antibiotic properties. For the purposes of this research, the chalcones are the basis for the synthesis of pyrroles. Lamellarin pyrroles have been synthesized from chalcones using electron cyclization chemistry of chalcones with glycine ethyl esters. The focus here is to generate pyrroles from chalcones en route to ynedienes. Ynedienes can be generated by the coupling of a halopyrrole with a terminal alkyne. These ynedienes will be examined for their ability to induce DNA cleavage via diradicals following the ynediene electrocyclization. The synthesis and purification of an O-protected hydroxyl chalcone has proven to be challenging. The scope of chalcones that can be utilized in the electrocyclization process has been expanded and will be discussed. The use of N-iodosuccinimide in the reaction process provides a halo-substituted pyrrole that will be coupled with terminal alkynes. The alkyne provides a handle for versatility in the next step(s) of the synthetic route. *In-silico* docking, as shown below in Figure 1, has helped form hypotheses for the results of future *in-vitro* testing of these analogs once they are available.

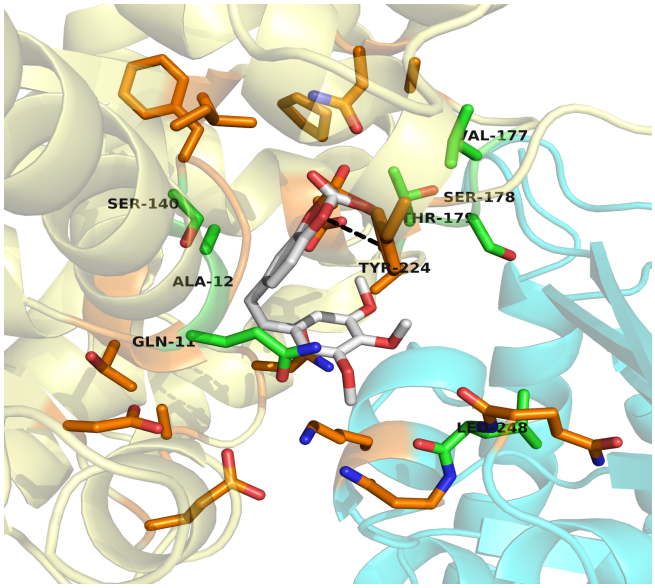

Figure 1. Interactions between bound CA-4P and the active site of tubulin-colchicine

1. Background

Cancer is the cause of approximately 600,000 deaths per year.[1] Even though this number has decreased over time, cancer remains recognized as one of the most detrimental diseases in the world.[2] Advances in STEM fields have led to the production of new medical technology and the isolation and synthesis of novel organic compounds with potential for anticancer activity. In 1989, Pettit and coworkers isolated Combretastatin A-4 or CA-4 (shown below in Figure 2) from the bark of the South African willow tree *Combretum caffrum*.[3] Shortly later that year, another group proved that CA-4 binds to the tubulin-colchicine protein active site and disturbs the microtubule domain hence inducing apoptosis or cell death.[4,5]

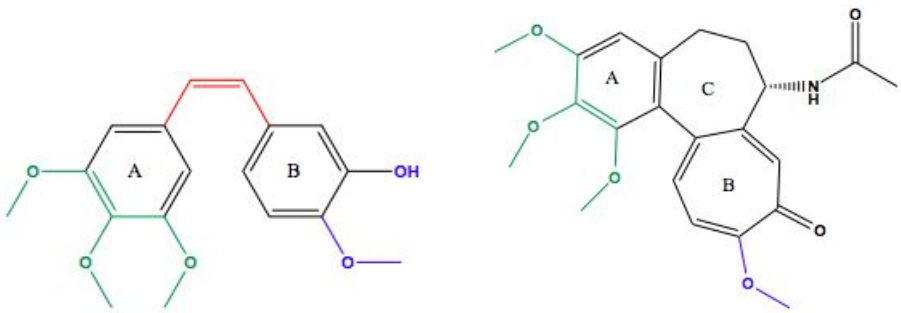

Figure 2. Structures of combretastatin A-4 or CA-4 (left) and colchicine (right)

Combretastatin A-4 (left) is a dihydrostilbenoid that is structurally related to colchicine (right) which binds to the active site within the tubulin-colchicine protein. CA-4 contains a fully conjugated pi-system with key structural features such as a trimethoxy A-ring highlighted in green, a *cis*-stilbene denoted in red, and a 3-hydroxyl and 4-methoxy groups on the B-ring shown in blue. These structural features promote its potent bioactivity in acting as a microtubule-destabilizing agent while being less toxic than colchicine.[5 6] The trimethoxy A-ring feature is a hydrogen bond acceptor thus containing the potential to interact with hydrogen bond donors such as the following amino acids: Tyrosine, Serine, and Threonine, depending on the environment of the active site as seen later in the *in-silico* docking section.

In clinical cancer therapeutic trials against multidrug resistant (MDR) cells, CA-4 has successfully interfered with the mitotic spindle's vascular function from interacting with the chromosome's kinetochores during the metaphase stage of mitosis, hence halting cell proliferation - the driving force for cancer.[3]

In-vitro, short exposure to CA-4 results in the profound long-term antiproliferative/cytotoxic effects against endothelial cells.[7] However, these effects prior to and during exposure do not impact quiescent, or in G_0 phase, endothelial cells.[7] *In-vivo*, studies have shown vascular shutdown followed by a 93% reduction of functional vascular volume with systemic drug administration.[7] However, due to CA-4's insolubility in water, transportation through the bloodstream is difficult. *In-vitro* at room temperature, CA-4 is soluble in solutions of 199.14 mM DMSO and 107.47 mM of EtOH, yet is water insoluble.[8] To be soluble *in vivo*, 5% DMSO, 50% PEG 300 and deionized water must be added to CA-4 promptly after mixing.[8] A phosphorylated version of CA-4, called CA-4P shown below in Figure 3, has been applied in human trials on patients with advanced cancer refractory to standard therapy.

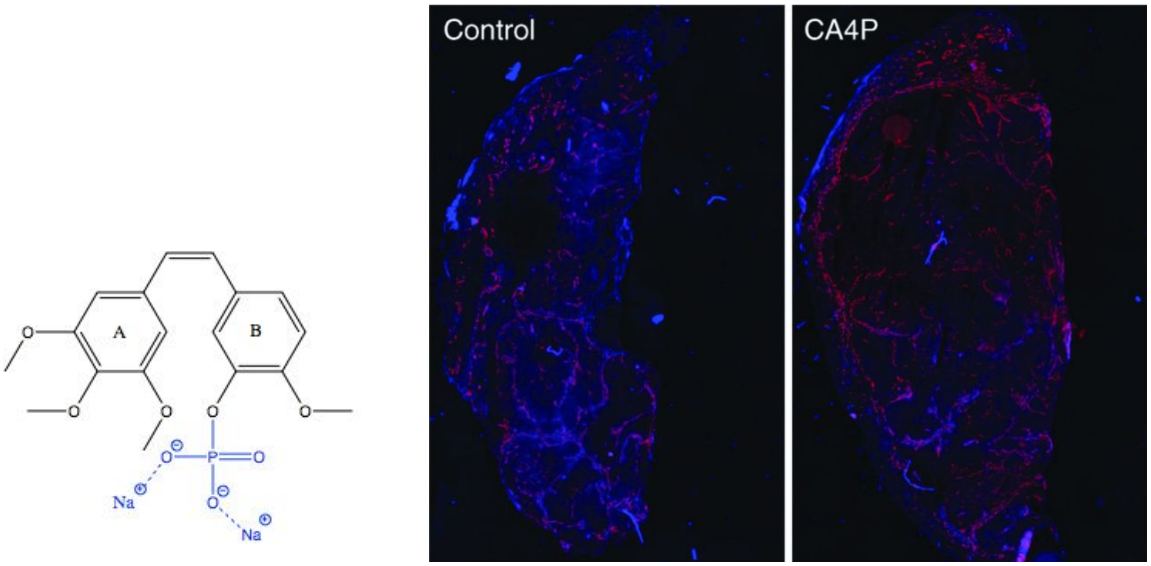

Figure 3. Structure and activity of combretastatin A-4 Phosphate (CA-4P) in tumors

Structurally, the only difference between CA-4 and CA-4P is a phosphate group (PO_4^{3-}) in the place of the hydrogen atom of the reactive 3-hydroxyl. Dissimilar from its unphosphorylated version, CA-4P is soluble *in-vitro* at room temperature when dissolved in 63.59 mM of water yet insoluble in solutions of DMSO or EtOH.[9] On the other hand, CA-4P is soluble *in-vivo* when a solution of saline and 5% Na_2CO_3 are added to the compound immediately after mixing.[9] The results provided anti-tumor activity in patients with ovarian, esophageal, small-cell lung cancer, and melanoma preventing the existing tumors from recruiting more blood vessels and initiating angiogenesis as shown on the right in Figure 3 where the red lines represent the unrecruitable blood vessels due to CA-4P .[9,10]

2. Introduction

The purpose of this research is to synthesize lamellarin pyrrole analogs from the chalcone derivatives of CA-4 and to produce biologically enhanced and more feasible anticancer compounds. This research consists of two foci. The target for the first focus is to ultimately increase the solubility and bioactivity of CA-4 analogs. This occurs by converting CA-4 into a variety lamellarin pyrrole intermediates in order to halt the rapid proliferation and overproduction of cells resulting in cancerous tumors. Within this focus, the binding activity of a key structural feature of CA-4, the trimethoxy feature of the A-ring, will also be tested both *in-vitro* and *in-silico*. The purpose for the second focus is to induce DNA cleavage via predicted Myers-Saito and Bergman electrocyclizations from a lamellarin pyrrole alkyne analog. This has the potential to prevent the translation of a mutated protein which can result in the formation of cancer.[10] A general scheme representing both foci are is shown below in Figure 4 as red and blue, respectively.

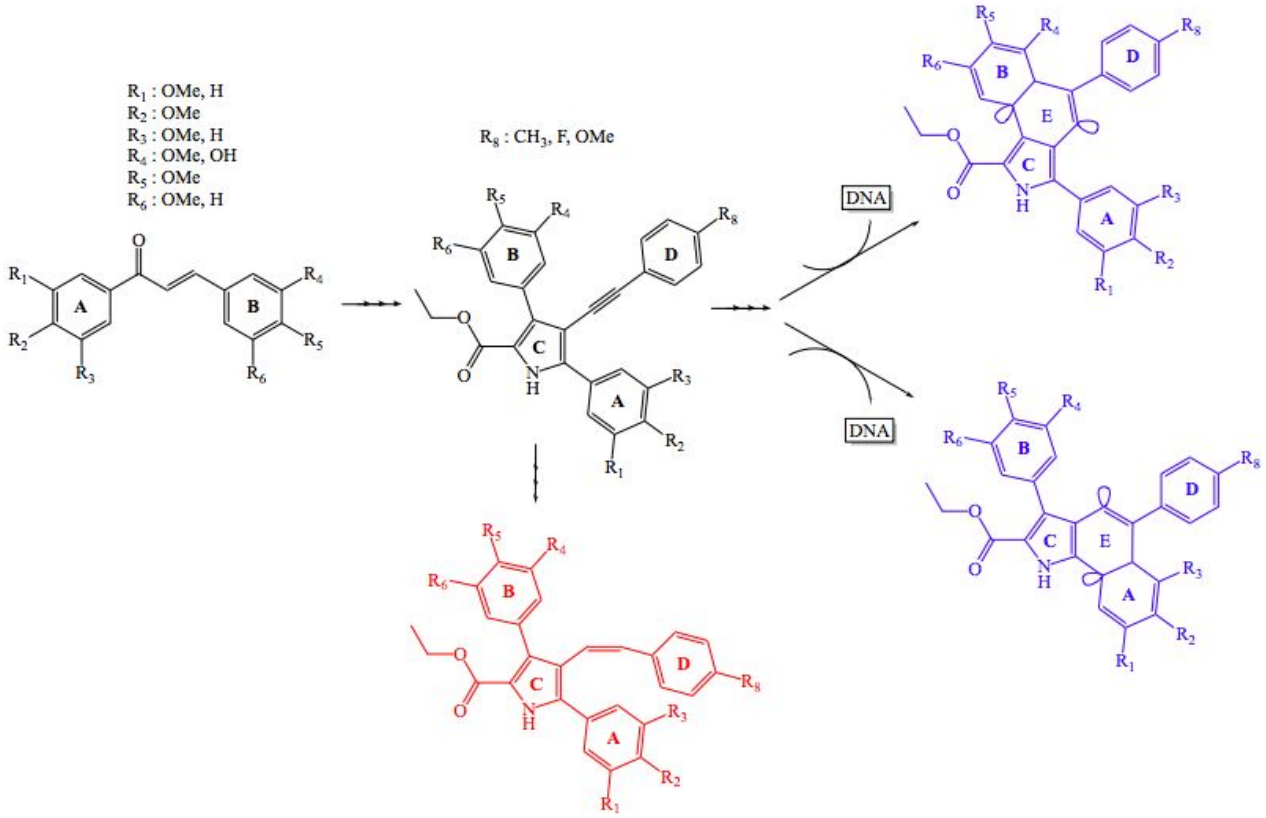

Figure 4. Generic products for both foci

Previous research in the Holt Lab has primarily focused on synthesizing target analogs of CA-4 to bind to the tubulin-colchicine protein and inhibit cell division. In current research, the lab is now producing a mix of lamellarin and CA-4 analogs. The former is a polycyclic marine pyrrole alkaloid and is defined by a central pyrrole core substituted at all positions with aromatic compounds as shown below in Figure 5 denoted in red.[11,12] These compounds have also shown activity in viral research.[11]

There are a variety of slightly different lamellarins with different structures and functions. For example, the Reddy Research Group synthesized lamellarin analogues which inhibit HIV-1 in cell culture.[7] The majority of lamellarin pyrroles are comprised with characteristics of strong biological activity that assist in the reversal of multidrug resistance in addition to strong proapoptotic effects through the inhibition of human topoisomerase I.[5] The lamellarin iodopyrrole created during the synthesis of producing lamellarin D is shown below in Figure 5 on the left. It is the most viable structure to undergo processes against MDR cancer cells when substituted with polar hydroxyl and methoxy groups at R_1 and R_2 as shown in lamellarin D on the right with such groups denoted in blue. While some analogs of this intermediate may result in an increase in solubility, others may be more susceptible to undergoing electrocyclization processes.

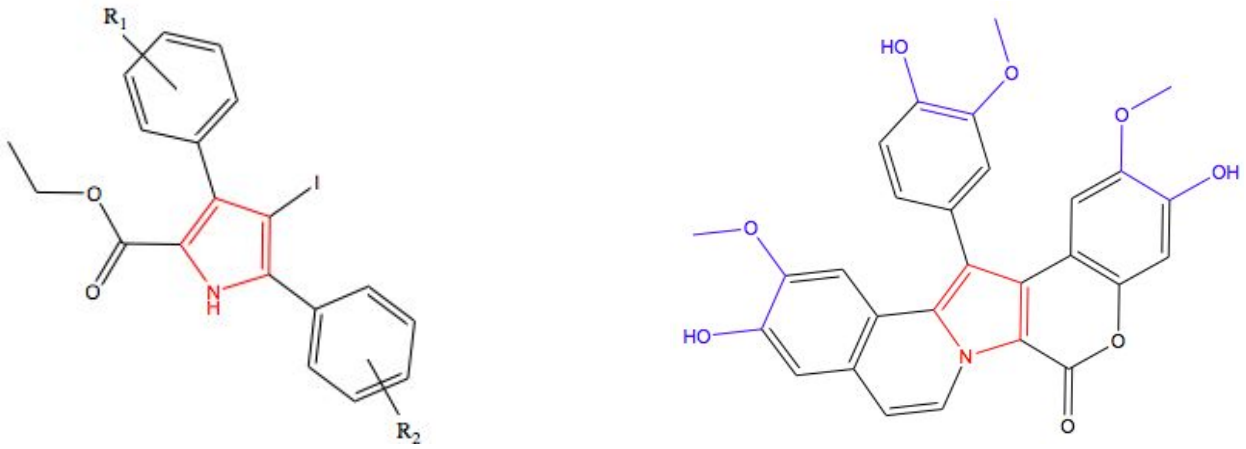

Figure 5. Structures of lamellarin iodopyrrole (left), lamellarin D (right)[13]

Lamellarins have strong biological potency due to its 3,4-diarylpyrrole core being an aromatic, five-membered nitrogenous ring shown above in red. The selectivity in binding tightly into the hydrophobic pocket of tubulin-colchicine is said to be determined by the trimethoxy feature of the A-ring of CA-4. This feature will be varied and tested both *in-silico* and *in-vitro* in order to determine whether it is truly necessary or if it could be modified for higher activity.

In hopes to further increase the solubility of these analogs the lamellarin pyrrole analogs will be coupled with a variety of terminal alkynes such as the following: *p*-tolylacetylene, 4-fluorophenylacetylene, 4-ethynylanisole. These alkynes will be coupled with the lamellarin iodopyrroles via Sonogashira coupling.

The fluorinated alkyne may assist in penetration of the blood brain barrier (BBB) to access brain tumors.[13,14] Fluorinated compounds have been used in radiopharmaceuticals specifically for assisting brain imaging. By freely diffusing through the intact BBB and remaining trapped in the neuronal tissue, positron emission tomography (PET) or single-photon emission CT (SPECT) scans may be collected. This is possible because fluorine has a similar Van Der Waals radii as hydrogen causing the C-F bond to mimic the biological behavior of C-H. According to Gouverneur, organofluorine compounds show benefits on ADME processes (absorption, distribution, metabolism, and excretion) in addition to providing more atom-interaction based properties such as distinct conformational and stereoelectronic properties, modulation of the pKa values of neighboring atoms, and intermolecular interactions, such as hydrogen bonding and dipole interactions with protein residues due to the high electronegativity of fluorine.[13]

These alkynes would undergo a selective reduction into a *cis*-alkene as this confirmation has been proven to be more thermodynamically stable in the tubulin-colchicine binding sites in comparison to the *trans*-alkene as seen with the low energy conformation provided by both CA-4P and CA-4 *in-silico*.[15] A generic scheme for the stepwise synthesis and product outcomes for the first focus are shown below in Scheme 1.

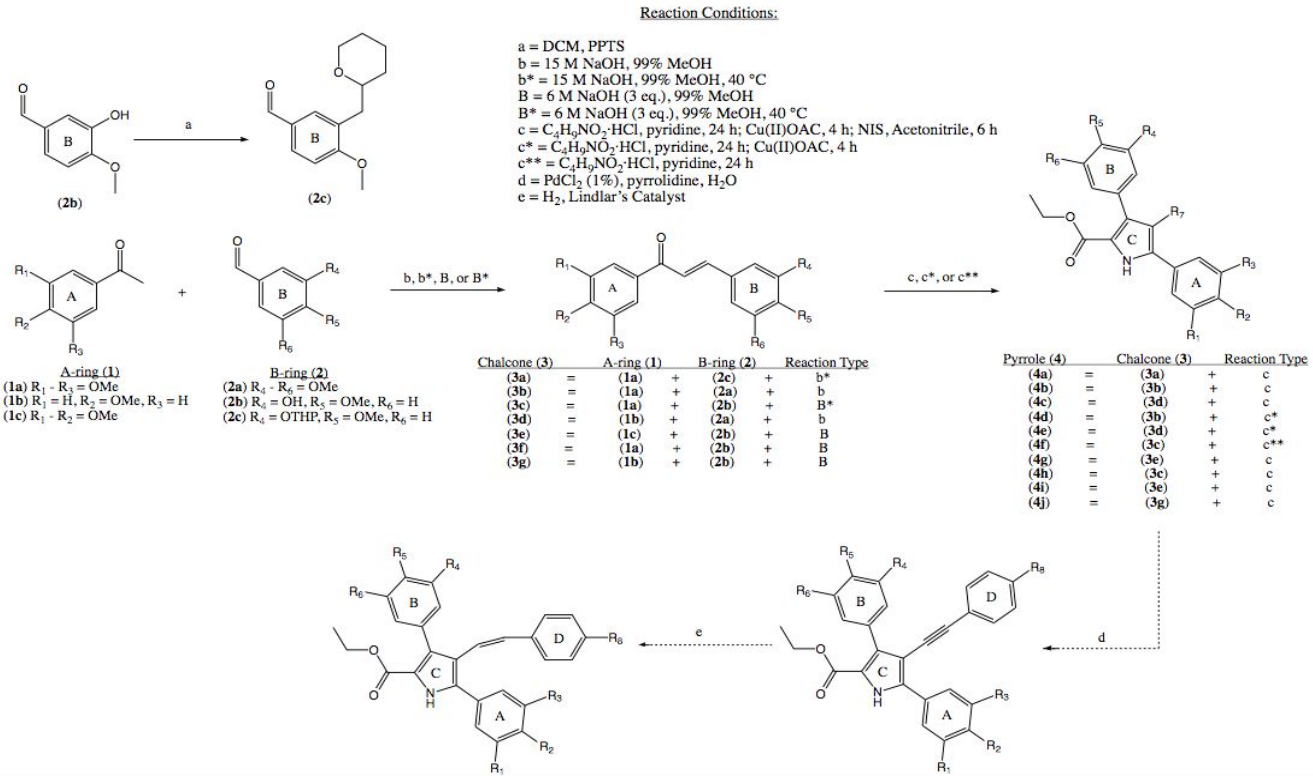

Scheme 1. On-going synthesis of first focus

In addition to deriving compounds to attach to the tubulin-colchicine protein to disrupt cell division, this research further endeavors into the potential cleavage of DNA helices. The overall purpose of this project is to prevent mutated vital proteins from being translated and activated in a cell thus containing the potential to expedite the rate of the cell cycle and produce tumors. By using the most electron-abundant intermediate, the lamellarin pyrrole alkyne shown below in Figure 6, DNA cleavage may be induced by having it mimic processes similar to that of the Myers-Saito and Bergman electrocyclizations of the enediyne family.

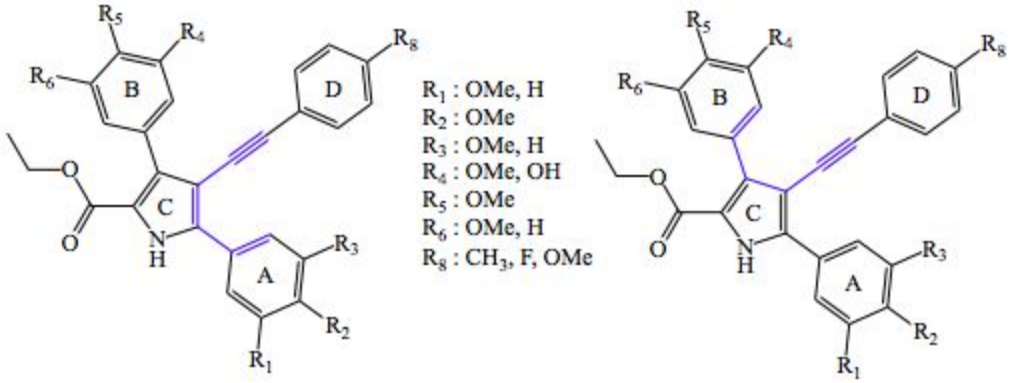

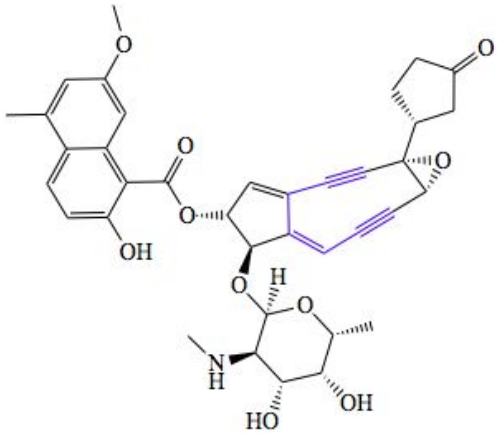

Figure 6. Lamellarin pyrrole alkyne (top) and neocarzinostatin chromophore or NCS (bottom)

Even though other members of the enediyne family, such as calicheamicins, esperamicin, and dynemicins, are proven to be more biologically active in anticancer and antitumor research, neocarzinostatin (NCS) is the compound which most closely envelops the essence of the ynediene functionality contained within the lamellarin pyrrole structure. There are two distinct electrocyclization processes that occur within the enediyne family. Most enediynes, like calicheamicin, esperamicin, and dynemicin undergo Bergman cyclizations forming 1,4-benzenoid diradicals on the same ring, while due to the presence of two sigma bonds between the double and triple bonds instead of one, NCS cyclizes via the Myers-Saito process. The latter forms two radicals on separate rings: one on a six-membered ring and the other on a five-membered ring. Due to the lack of electrons within the lamellarin pyrrole alkyne, a process similar to Bergman electrocyclization is predicted to occur thus making it necessary to look at both NCS and calicheamicin structures and electrocyclization processes.

NCS is a naturally occurring antibiotic with antitumor activity and was isolated from *Streptomyces carzinostaticus*. This molecule consists of a 1:1 ratio between its two moieties: the NCS apoprotein (shown below in green in Figure 7) and the NCS chromophore.[20, 21] Ishida *et al.* discovered that all of the bioactive properties are located in the NCS chromophore shown above in Figure 6.[20] The properties that cause the bioactivity of the enediynes to be so unique is that they consist of a complex system composed of warheads (or diradicals), a delivery system, and a triggering device that allow for the diradicals to cleave DNA as shown below in Figure 7.[12]

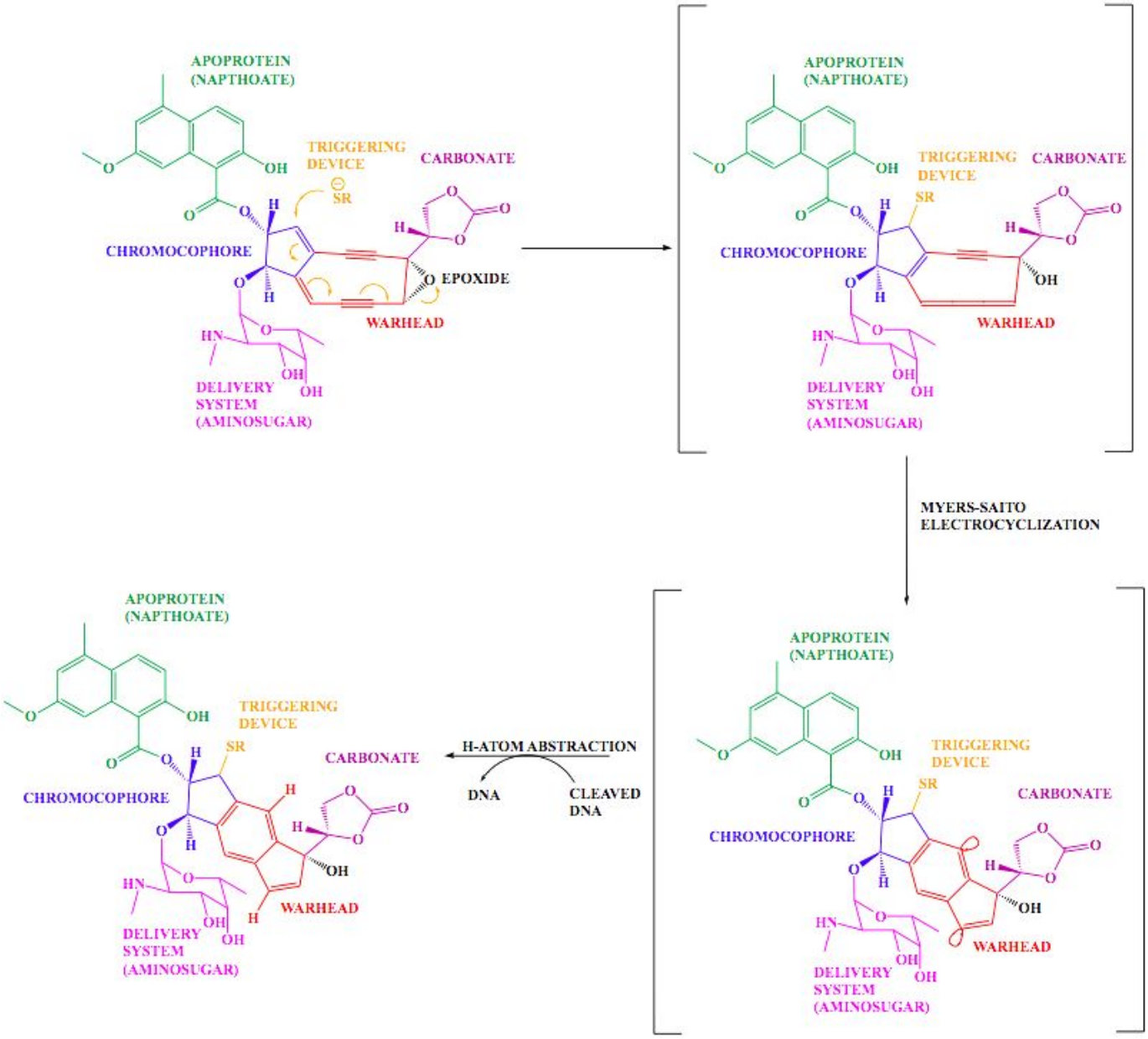

Figure 7. Neocarzinostatin myers-saito electrocyclization

Both Bergman and Myers-Saito electrocyclizations consist of a set of active, unstable warheads (shown above in red) and form the diradical complex produced from the enediyne. Each enediyne has a different delivery system (shown above in pink) each consisting of a specific amino sugar that takes the compound to its designated site on the DNA double helix called the restriction site. Another delivery system underconsideration is primarily made of sugars with exposed phosphate groups that will break apart once they have undergone metabolic processes, such as glucuronidation, and thus exposing the compound to the triggering device.The triggering device (shown in orange) destabilizes the locking device that holds the compound together and causes a cascade of reactions to occur forming the diradical warheads. The host DNA undergoes a modification by a methyltransferase enzyme which prohibits the triggering device from binding to the double helix thus causing the phosphodiester bonds of the mutated DNA to dismantle.[22]

The most electron abundant lamellarin pyrrole intermediate, being the coupled alkyne as shown previously in Figure 6, appears to be more structurally similar to NCS while hypothetically, seems to undergo Bergman electrocyclization to form heterocyclic diradicals on the same ring, like Calicheamicin. These radicals are predicted to be accessible and not restricted by steric hindrance. The radical orbitals colored in red shown on the A-E and B-E ring fusions are not within the conjugated pi-system of the fused heterocycle and is therefore perpendicular to the planarity of the A-E and B-E ring systems (Figure 8). The radical orbitals colored in blue is on a carbon with a double bond already in place. As the pi-orbitals are occupied, the position of this radical is predicted to be perpendicular to the pi-system and is, therefore, in the same plane as the A-E and B-E ring systems.

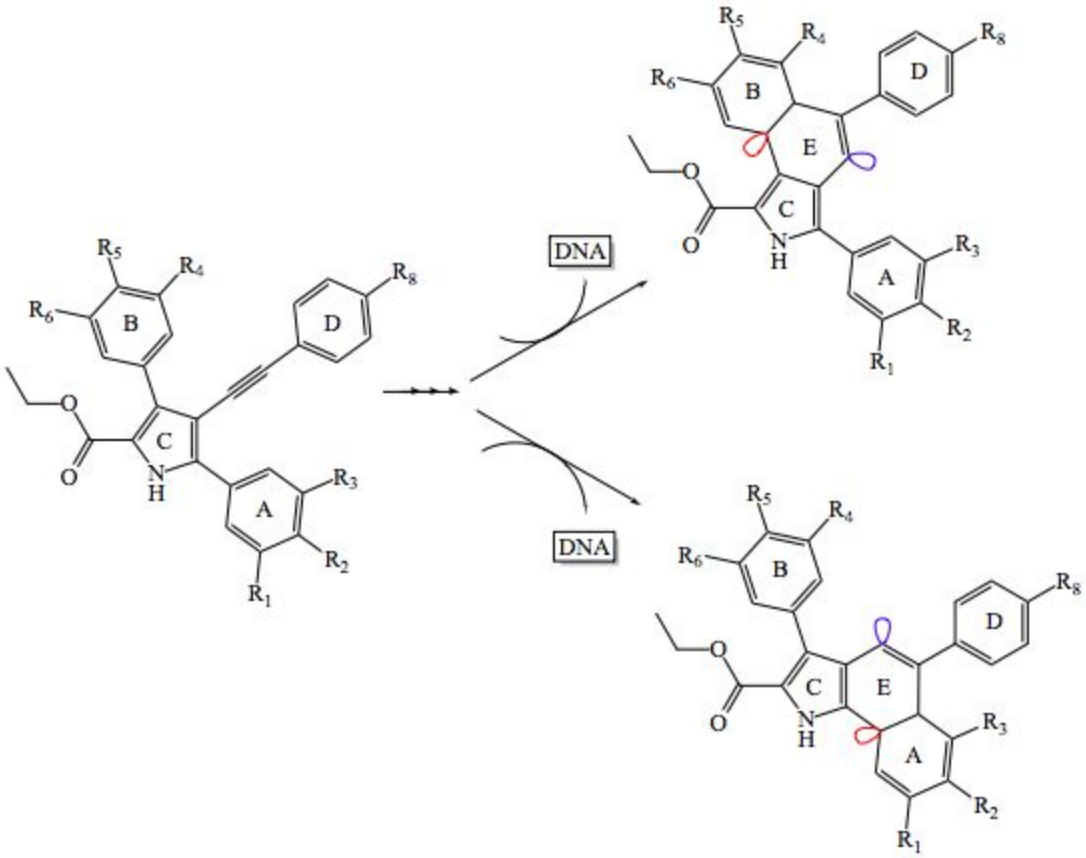

Figure 8. Diradical orientation in products

3. Results and Discussion

Results of isolating the precursors to the lamellarin pyrrole analog (halogenated or non halogenated) have been difficult to obtain. Initially, (*E*)-3-(3-hydroxy-4-methoxyphenyl)-1-(3,4,5-trimethoxyphenyl)prop-2-ene-1-one (**3c**) did not form as the acidity of the B-ring 3-hydroxyl group was higher than that of the ketone of the A-ring, as depicted in Figure 9, thus interfering with the chalcone mechanism.

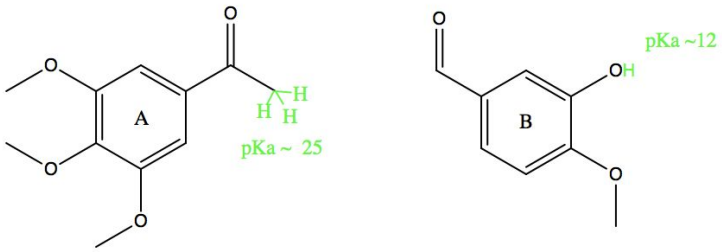

Figure 9. pK_a values of A-ring ketone and B-ring hydroxyl

Therefore, several protecting groups like ethoxyethyl ethers, Mukaiyama's reagent, trimethylsilyl ethers, and OTHP were taken under consideration to replace the 3-hydroxyl on the B-ring in order for the chalcone properly form. The latter option of an OTHP group was selected as it is base insensitive, utilizes groups which upon removal will not affect the methoxy substituents, and has a long half-life. On the other hand, OTHP protecting groups are column sensitive and hard to recover post purification. Next, Dr. Jalisa Ferguson, the Holt Lab's GlaxoSmithKline post-doctoral fellow, discovered that 3 molar equivalents of base could assist in the proper formation of the chalcone. Thus far, the chalcones have provided higher average percent yields ranging from 70% - 95% as shown in the graph of percent yields vs. chalcone type reaction conditions below in Scheme 2.

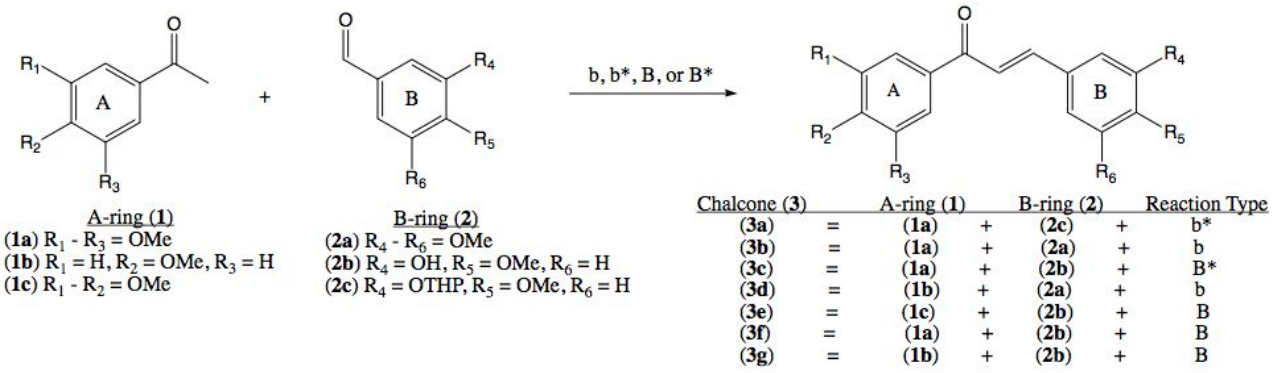

Chalcone (3)		A-ring (1)		B-ring (2)		Reaction Type
(3a)	=	(1a)	+	(2c)	+	b*
(3b)	=	(1a)	+	(2a)	+	b
(3c)	=	(1a)	+	(2b)	+	B*
(3d)	=	(1b)	+	(2a)	+	b
(3e)	=	(1c)	+	(2b)	+	B
(3f)	=	(1a)	+	(2b)	+	B
(3g)	=	(1b)	+	(2b)	+	B

Scheme 2. Generic reaction scheme of chalcone synthesis

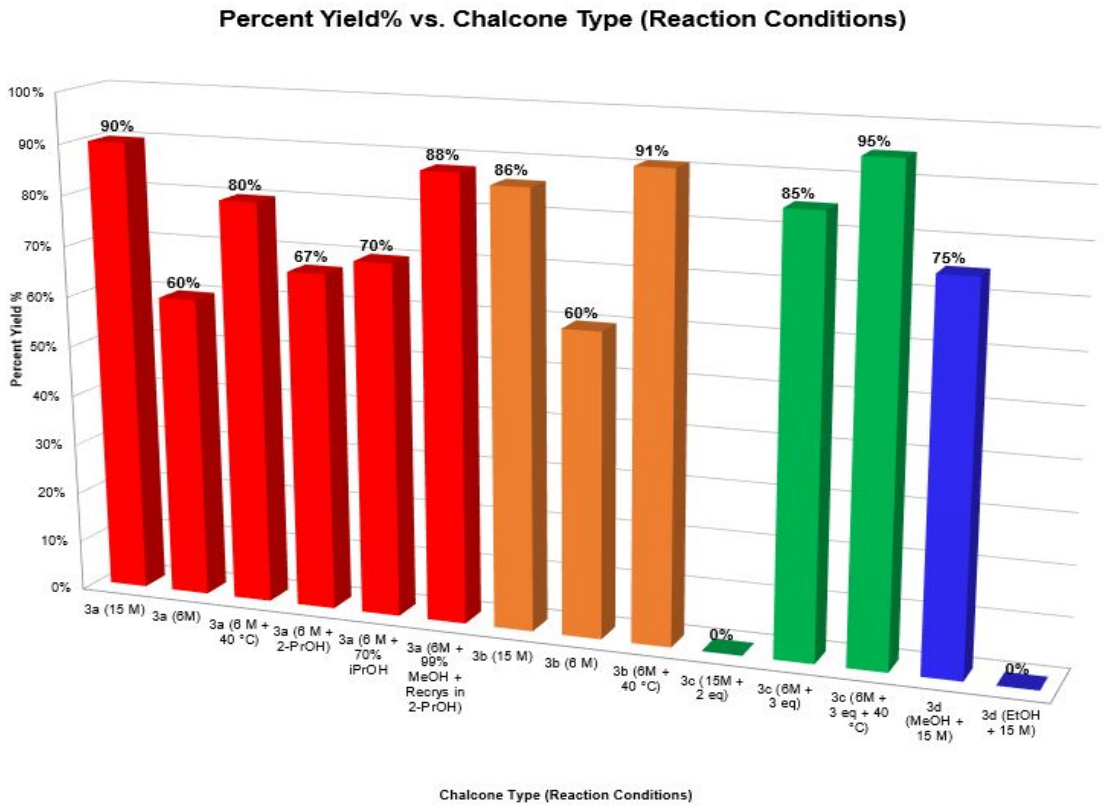

Figure 10. Percent yield vs. chalcone type reaction conditions

The outcomes of the reaction shown above in Scheme 2 are represented in the bar-graph shown in Figure 10. The chalcone reaction types providing the highest percent yields range from 75% to 96%. Chalcone (**3a**) depicted in red afforded the best results when reacting its A- and B-rings (**1a**) and (**2c**), respectively, under conditions type b with 15 M base. Chalcone (**3b**) depicted in orange afforded a percent yield of 91% when reacted under conditions type b* with 6 M base, MeOH, and refluxing at 40 °C. Chalcone (**3c**) shown in green provided the highest percent yield of 95% under conditions type b with 3 molar equivalents of 6 M base refluxing at 40 °C. Chalcone (**3c**) provided no product when adding 2 molar equivalents of 15 M base to its reactants. Chalcone (**3d**) shown in blue offered its highest percent yield (75%) under conditions type b with a 15 M base and solvent of MeOH. When solvents were switched from MeOH to EtOH, no product was provided. In general, the most effective reaction conditions were using a 6 M base solution, MeOH, and reflux at 40 °C and were observed for chalcones (**3a**) - (**3c**). These conditions provided an 80% yield for chalcone (**3a**), and the highest percent yields observed for chalcones (**3b**) and (**3c**), 91% and 95% respectively. Yet when using reaction conditions of 6 M base solution with MeOH alone, chalcones (**3a**) and (**3b**) both offered their lowest percent yields, 60%. Chalcones with hydroxyl groups like chalcone (**3c**), thrived when using 3 molar equivalents of a lower molarity of base, like 6 M. Percent yields for chalcones (**3e**) and (**3f**) have not yet been collected.

Similar methodological investigations are being performed on the synthetic procedures of the lamellarin iodopyrrole intermediate. Currently, reactions c, c*, and c** represent each cumulative step of the lamellarin iodopyrrole reaction. This data will be used to determine (1) the step in which the highest yield of product is recovered and (2) the best intermediate to undergo purification to maintain the highest yield possible (Scheme 3).

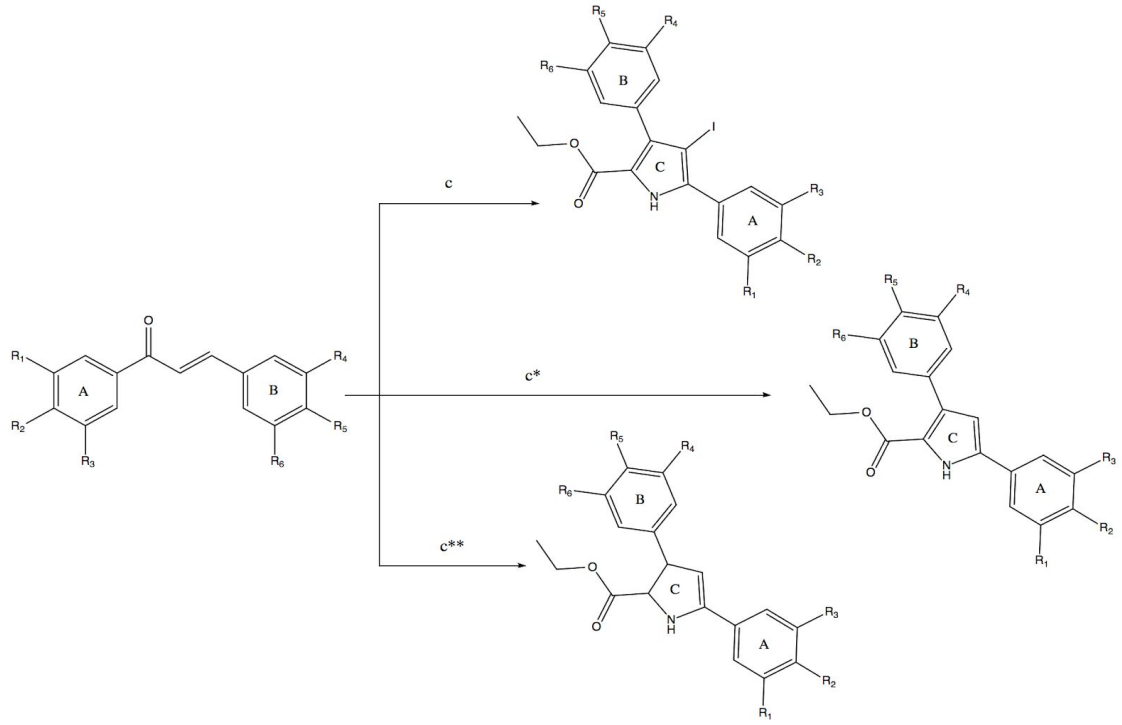

Scheme 3. Stepwise pyrrole reactions

c = Glycine ethyl ester hydrochloride, pyridine, copper (II) acetate, NIS, acetonitrile; c* = Glycine ethyl ester hydrochloride, pyridine, copper (II) acetate; c** = Glycine ethyl ester hydrochloride, pyridine

Initially, the 3-step one-pot synthesis was causing problems in percent recovery and was difficult to confirm via ^{1}H-NMR. Once the halogenation step was removed, a non-halogenated pyrrole was expected to be more visual in ^{1}H-NMR due to the presence of an extra hydrogen, yet this was still unclear. Reactions with glycine ethyl ester hydrochloride, pyridine, and chalcone will be worked up with the expectations of producing a dihydropyrrole as shown above in Scheme 3 following procedures c**.

4. Computational Docking:

Docking these compounds in the active site of the tubulin-colchicine protein allows for the analysis of amino acid interactions between the protein and the ligand in addition to the comparison of K_D values with that of CA-4P, the ligand with the lowest energy conformation, hence, the best binding affinity seen thus far. More specifically, interactions with the glycine ethyl ester handle (purple), B-ring methoxy and hydroxyl groups (blue), halogen (pink), pyrrole core (red), and trimethoxyacetophenone binding feature (green) were identified in order to further determine the significance of their activities. Moreover, these analogs allow for another scope of focus: to test the activity of the binding site for the trimethoxyacetophenone feature highlighted in green. Previous research has stated the importance of this feature to serve as a "key" in binding into the site; however, this project will test and extrapolate as to why this may be.

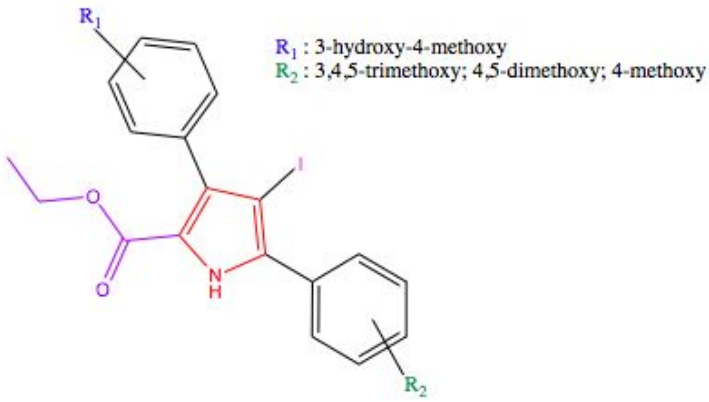

Figure 11. Lamellarin pyrrole intermediate variations

Analogs of the halogenated lamellarin pyrroles were prepared *in-silico* and docked into the tubulin-colchicine protein in order to identify amino acid interactions with the specific functional groups of each lamellarin pyrrole intermediate analog. Software including Chemdraw, Chem3D, AutoDock Tools, AutoDock Vina, and Pymol were utilized to dock the ligands into the tubulin-colchicine protein (ID# 1SA0) as shown below in Figure 12.

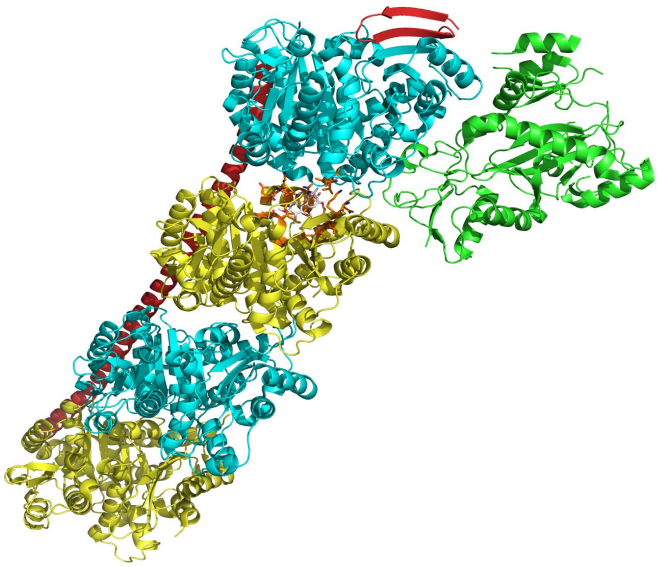

Figure 12. Protein ID #1SA0 with colchicine docked in the active site

As seen in the image above, there are two alpha (yellow) and beta (blue) chains and therefore, two binding sites per protein. Since these chains contain the same amino-acid composition, the following experiment focuses only on one. Each ligand appears to be docked in the active site shared between the alpha and beta chains as shown below in Figure 13.

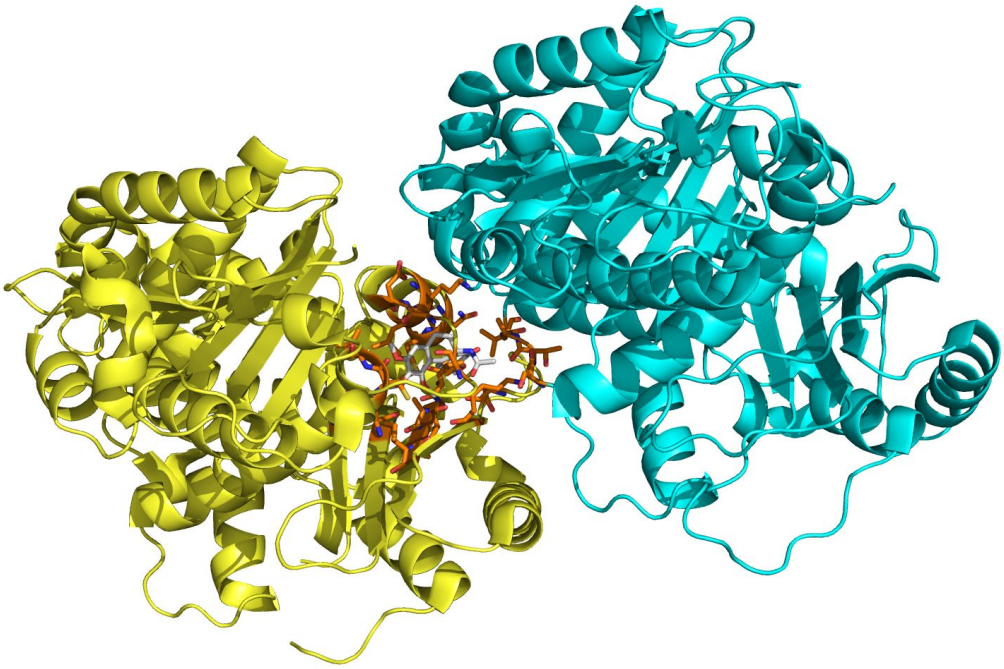

Figure 13. Colchicine docked in the active site between the alpha and beta chains of tubulin-colchicine (ID #1SA0)

The following figure, Figure 14, shows the binding interactions of CA-4 and the surrounding amino acid residues in the tubulin-colchicine protein. These interactions are then compared with those of other ligands (including chalcones, pyrroles, and coupled alkynes) for the first focus. The selected ligands vary the quantity of methoxy groups on the A-ring, the interactions between the ligand and amino acids of the protein within 4 angstroms of the ligand, the ΔG (kcal•mol^{-1}) and K_D (μM). Each amino acid residue located within 4 angstroms of the ligand are denoted in orange, those interacting via Van Der Waals forces are represented as sticks in green, hydrogen bonds are represented as dashed lines in black, pi-pi bonds as multiple dashed lines (usually 6) in red, and pi-cation bonds as dashed lines in blue.

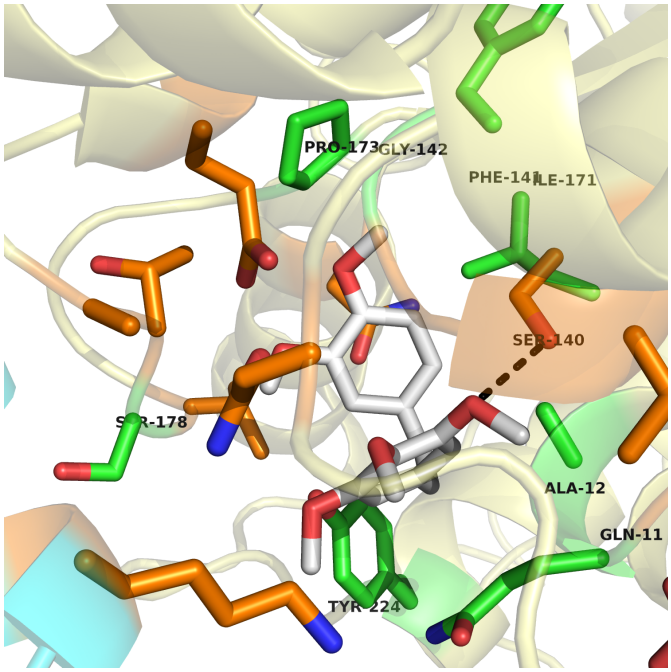

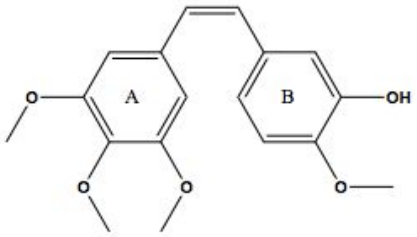

Figure 14. CA-4 docked in tubulin-colchicine (ID# 1SA0)

The K_D and ΔG (Gibbs Free Energy) for the lowest energy conformation of the 9 modes offered by Autodock Vina for CA-4 as a ligand in tubulin-colchicine was 92.5 µM and -5.5 kcal•mol^{-1}. Moreover, a hydrogen bond denoted in a black dashed line is observed between the amino acid residue Serine 140 and the Oxygen atom of the 3- or 5-methoxy on the A-ring which acts as a hydrogen bond acceptor.

These results differ greatly from CA-4P with a K_D and ΔG of 1.15 µM and -8.1 kcal•mol^{-1}. A hydrogen bond still appears yet is between the oxygen of the phosphate group on the B-ring and Tyrosine 224. Perhaps this is the best affinity observed throughout these ligands due to its small and flexible structure in addition to its proper "fit" within the binding site as seen below in Figure 15.

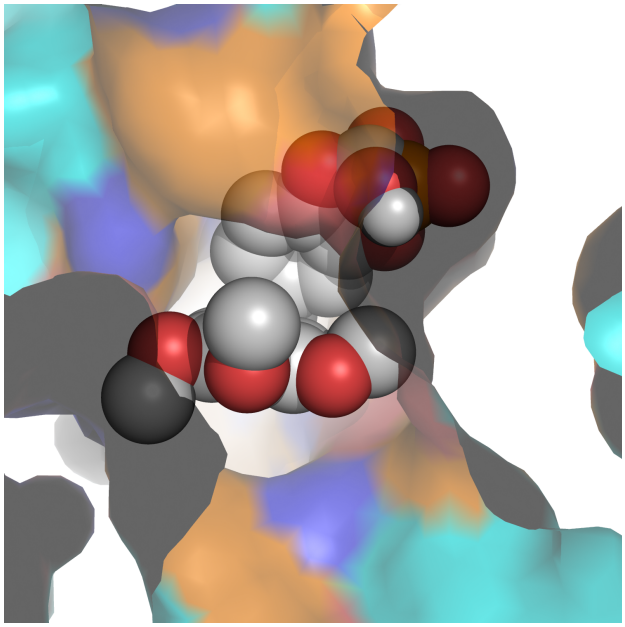

Figure 15. Van Der Waals forces of CA-4P docked into surface model of tubulin-colchicine (ID# 1SA0)

Colchicine offered 6 binding modes with a lower affinity of 6.2 µM and a ΔG of -7.1 kcal•mol^{-1}. Another hydrogen bond is observed yet between the carbonyl oxygen atom on the B-ring and Glutamine 11.

When the Van Der Waals radii of the chalcones are compared with that of CA-4P, the latter still has the best fit within the active site of the protein. Chalcone **3c** contains a pi-stacking interaction between the B-ring and the phenol of Tyrosine 224 in addition to a K_D of 3.74 µM and a ΔG of -7.4 kcal•mol^{-1}. While this is better than the binding affinity of colchicine, it is not as fitting as the following chalcone.

Chalcone **3e**, surprisingly, has a better binding affinity than the chalcone with the trimethoxy feature on the A-ring. The dimethoxy chalcone allows for a K_D of 2.67 µM and a ΔG of -7.6 kcal•mol^{-1} in addition to a hydrogen

bond between the hydroxyl group of the B-ring and the hydroxyl of Threonine 145 and a pi-stacking interaction between the A-ring and the phenolic ring of Tyrosine 224.

The chalcone with a 4-methoxy feature on the A-ring, chalcone **3g**, provides a K_D of 3.16 μM and a ΔG of -7.5 kcal•mol^{-1} in addition to a hydrogen bond between the hydroxyl group of the B-ring and the oxygen atom of the carbonyl of Asparagine 228 and a pi-stacking interaction between the B-ring and the phenol of Tyrosine 224.

The lamellarin iodopyrrole intermediates, on the other hand, are much larger and less flexible than chalcones of the combretastatin analogs and were hypothesized to have a worse binding affinity than that of CA-4P. This was confirmed when the trimethoxy (**4h**), dimethoxy (**4i**), and 4-methoxy (**4j**) lamellarin iodopyrroles were docked. Lamellarin iodopyrrole **4h** demonstrated a K_D of 130 μM and a ΔG of -5.3 kcal•mol^{-1} and only offered 3 conformational modes. A hydrogen bond between the hydroxyl group of Serine 140 and the hydroxyl group of the B-ring seemed to establish this mode as it did not appear in any of the other conformations.

Lamellarin iodopyrrole **4i** offered an improved binding affinity of 8.69 μM and a ΔG of -6.9 kcal•mol^{-1} yet only provided 2 conformational modes. The best mode established a hydrogen bond between Tyrosine 224 and the amine hydrogen from the C-ring of the ligand. Furthermore, this conformation also allowed for a new interaction observed between the positively charged nitrogen atom of the Lysine 254 residue acting as a monopole to the quadrupole pi-system of the B-ring.

Lamellarin iodopyrrole **4j** with the 4-methoxy feature on the A-ring surprisingly offered more more conformational modes than the latter pyrrole in addition to a better binding affinity than the analog with the trimethoxy feature: K_D = 4.42 μM and a ΔG = -7.3 kcal•mol^{-1}. This analog offers two hydrogen bonding interactions between the hydroxyl group of Tyrosine 224 and the amine hydrogen on the C-ring and hydroxyl group of Serine 140 and the hydroxyl group of the B-ring.

The last group of analogs that were tested were the lamellarin pyrrole alkynes. Only three analogs were tested *in-silico* with the trimethoxy feature on the A-ring and the 3-hydroxyl-4-methoxy feature on the B-ring where the functional groups of the coupled terminal alkyne varied between a methyl (analog **5a**), a fluorine (analog **5b**), and a methoxy (analog **5c**). These analogs are even larger than the lamellarin pyrroles, hence, further decreasing their binding affinities.

Analog **5a** offered 3 conformational modes and a K_D of 22900 μM and a ΔG of -3.6 kcal•mol^{-1} along with two hydrogen bonding interactions between the 4-methoxy oxygen on the A-ring and Glycine 146 and the 3- or 5-methoxy feature on the A-ring and Serine 146. The next analog, **5b**, provided 4 conformational modes and a K_D of 156000 μM and a ΔG = -7.3 kcal•mol^{-1} with the same interactions as the latter analog except for the hydrogen bond with Glycine 146. Lastly, analog **5c** offered 2 conformational modes and best binding affinity for the lamellarin pyrrole alkynes thus far with a K_D of 28800 μM and a ΔG of -2.1 kcal•mol^{-1}. Moreover, it provided the highest amounts of interaction thus far including two hydrogen bonds between the 3- and 4- methoxy oxygens and Serine 140 and Glycine 10, respectively, in addition to a pi-stacking interaction between the phenolic ring of Tyrosine 224 and the alkyne or D-ring.

These data have allowed for further predictions regarding the results of the *in-vitro* assays which will follow this project. The lamellarin pyrrole alkyne with the most interactive species, analog **5c**, is predicted to have the highest activity in inducing cell death within the MTT assay even though it is among the ligands with the worst binding affinities thus far. Meanwhile, the dimethoxy featured A-rings of both the chalcones and lamellarin pyrroles are predicted to have the most reactivity also due to the amounts of interactions between these ligands and the amino acid residues within the tubulin-colchicine protein.

5. Experimental

5.1 Computational Docking

Computational docking was performed by first creating the ligand in ChemDraw then transferring it to Chem3D. This file was then opened in Autodock Tools where the root was detected and bond torsions were identified. Next, the protein ID# SA0 was fetched from the protein data bank in PyMol and then transferred to Autodock Tools for further modifications including the deletion of water, the addition of hydrogen atoms, the merging of non-polar hydrogen atoms, the removal of all excess atoms and ions, and the computation of Gasteiger charges. At this point, the protein

was selected as a macromolecule and the grid box was defined in the given binding site between the alpha and beta chains. The correct output files were created and Autodock Vina was ran.

These output values represent the ΔG (kcal•mol^{-1}) of each of the 3 to 9 different modes provided with mode 1 representing the lowest energy conformation of the ligand. These values were produced via Lamarckian genetic algorithms by Autodock Vina and were converted to K_D values (μM) by the using the following formula provided by Autodock:

$$K_D = e^{\Delta G/RT}$$

On the left side of the equation is the constant of dissociation (KD) while on the right is the exponential constant (2.718) raised to the power of Gibbs Free Energy constant (ΔG) divided by the gas constant (R = 1.987•10^{-3} kcal•mol^{-1}•K^{-1}) multiplied by T (temperature in Kelvins). The given negative ΔG (kcal•mol^{-1}) that is provided is plugged into the equation along with the gas constant R = 1.987 x 10^{-3} kcal•mol^{-1}•K^{-1} and T = 298 K.

The output file was opened in PyMol and the mode with the lowest energy conformation was selected. The amino acids within 4 angstroms were identified and represented as sticks. In Autodock, this output file was also opened and the interactions between the protein and ligand were identified and displayed in PyMol. Each amino acid interacting via Van Der Waals forces were represented as sticks in green, hydrogen bonds were represented as dashed lines in black, pi-pi bonds as multiple dashed lines (usually 6) in red, and pi-cation bonds as dashed lines in blue. These images were sharpened via ray tracing in order to have a higher resolution.

5.2 Organic Synthesis

*4-methoxy-3-((tetrahydro-2H-pyran-2-yl)oxy)benzaldehyde (**2c**)*

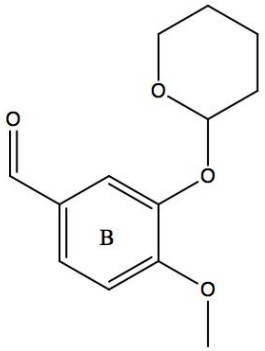

3-hydroxy-4-methoxybenzaldehyde (**2b**) (6.44 g, 42.3 mmol, 6.66 equiv) and 3,4-dihydro-2*H*-pyran (23.2 mL, 25.4 mmol, 4.00 equiv) was placed in a 1-neck round-bottom flask with dichloromethane and pyridinium *p*-toluenesulfonate ester (1.60 g, 6.35 mmol, 1.00 equiv) at room temperature for 15 h. The addition of minimal ice chips affected the formation of an oil-based product several minutes later. The reaction mixture was stirred for 16 h followed by a liquid-liquid extraction with saturated potassium carbonate (3 x 20 mL). The residue was dissolved in dichloromethane (15 mL), dried over anhydrous Na_2SO_4, filtered, and finally concentrated to dryness *in vacuo* which afforded the crude title
compound as a yellowish viscous oil which can be used for the next step without further purification (9.61 g, 96 %).

*(E)-3-(4-methoxy-3-((tetrahydro-2H-pyran-2-yl)oxy)phenyl)-1-(3,4,5-trimethoxyphenyl)prop-2-en-1-one (**3a**)*

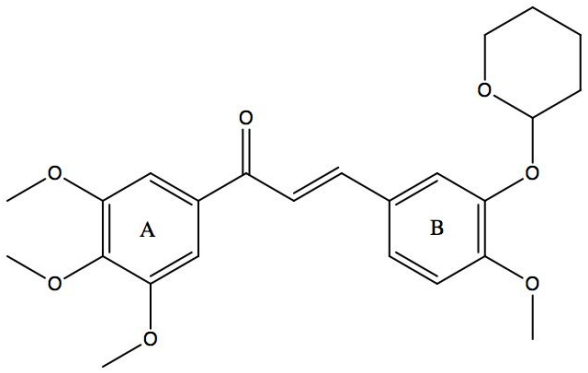

3,4,5-trimethoxyacetophenone (**1a**) (0.11 g, 0.53 mmol, 1.06 equiv) and 4-methoxy-3-((tetrahydro-2H-pyran-2-yl)oxy)benzaldehyde (**2c**) (0.12 g, 0.5 mmol, 1.00 equiv) were suspended in 99% MeOH (6.5 mL). The addition of 6 M NaOH (1.7 mL, 31 mmol, 2.00 equiv) affected the formation of a yellow precipitate a few minutes later. Reaction was stirred for 1 h followed by suction filtration and washing with 99% MeOH (3 x 10 mL). The residue was dissolved in dichloromethane (10 mL), dried over anhydrous Na_2SO_4, filtered, and finally concentrated to dryness in vacuo to yield the title compound as an yellow amorphous solid (0.18 g, 86%). NMR

*(E)-1,3-bis(3,4,5-trimethoxyphenyl)prop-2-en-1-one (**3b**)*

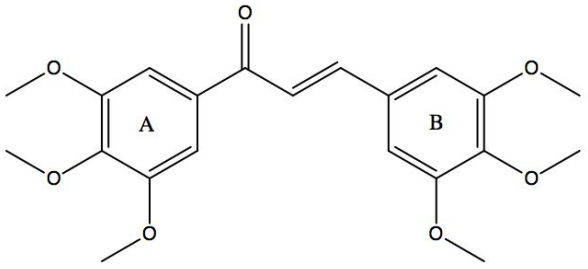

3,4,5-trimethoxyacetophenone (**1a**) (1.15 g, 5.3 mmol, 1.06 equiv) and 3,4,5-trimethoxybenzaldehyde (**2a**) (1.01 g, 5.0 mmol, 1.00 equiv) were suspended in 99% MeOH (6.5 mL) and heated to reflux to form a white solution. The addition of 6 M NaOH (1.7 mL, 31 mmol, 2.00 equiv) affected the formation of a yellow precipitate a few minutes later. Reaction was heated to 40 °C and refluxed for 1 h followed by suction filtration and washing with 99% MeOH (3 x 10 mL). The residue was dissolved in dichloromethane (10 mL), dried over anhydrous Na_2SO_4, filtered, and finally concentrated to dryness in vacuo to yield the title compound as an yellow amorphous solid (1.67 g, 84 %).

(E)-3-(3-hydroxy-4-methoxyphenyl)-1-(3,4,5-trimethoxyphenyl)prop-2-en-1-one (**3b**)

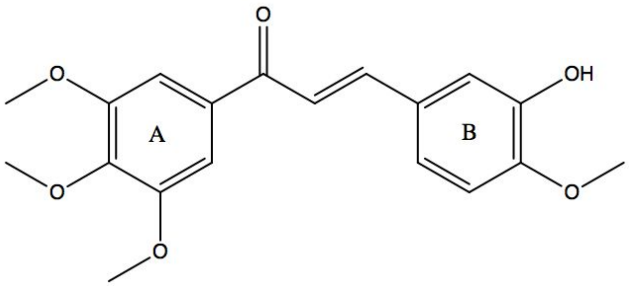

3,4,5-trimethoxyacetophenone (**1a**) (1.35 g, 6.4 mmol, 1 eq.) and 3-hydroxy-4-methoxybenzaldehyde (**2b**) (1.03 g, 6.8 mmol, 1.06 eq.) were suspended in 99% MeOH (10 mL) and heated to reflux to form a white solution. The addition of 6 M NaOH (3.2 mL, 19.2 mmol, 3 eq.) affected the formation of a yellow precipitate a few minutes later. Reaction was heated to 40 °C and refluxed for 1 h followed by suction filtration and washing with 99% MeOH (3 x 10 mL). The residue was dissolved in dichloromethane (10 mL), dried over anhydrous Na_2SO_4, filtered, and finally concentrated to dryness in vacuo to yield the title compound as an yellow amorphous solid (1.70 g, 83 %). Unconfirmed via spectral data.

*(E)-1-(4-methoxyphenyl)-3-(3,4,5-trimethoxyphenyl)prop-2-en-1-one (**3c**)*

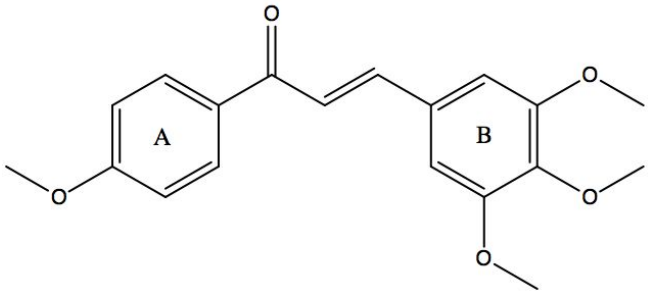

4-methoxyacetophenone (**1b**) (0.08 g, 0.5 mmol, 1.00 equiv) and 3,4,5-trimethoxybenzaldehyde (**2a**) (0.098 g, 0.53 mmol, 1.06 equiv) were suspended in 99% MeOH (6.5 mL). The addition of 6 M NaOH (1.7 mL, 31 mmol, 2.00 equiv) affected the formation of a yellow precipitate a few minutes later. Reaction stirred for 1 h followed by suction filtration and washing with 99% MeOH (3 x 10 mL). The residue was dissolved in dichloromethane (10 mL), dried over anhydrous Na_2SO_4, filtered, and finally concentrated to dryness in vacuo to yield the title compound as an yellow amorphous solid (0.09 g, 75 %).

*(E)-1-(3,4-dimethoxyphenyl)-3-(3-hydroxy-4-methoxyphenyl)prop-2-en-1-one (**3e**)*

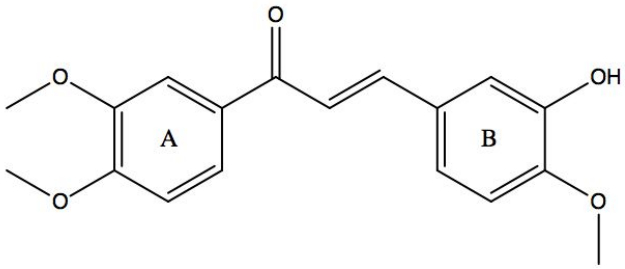

3,4,5-trimethoxyacetophenone (**1a**) (1.15 g, 6.4 mmol, 1 eq.) and 3-hydroxy-4-methoxybenzaldehyde (**2b**) (1.03 g, 6.8 mmol, 1.06 eq.) were suspended in 99% MeOH (10 mL) and heated to reflux to form a white solution. The addition of 6 M NaOH (3.2 mL, 19.2 mmol, 3 eq.) affected the formation of a yellow precipitate a few minutes later.

Reaction was heated to 40 °C and refluxed for 1 h followed by suction filtration and washing with 99% MeOH (3 x 10 mL). The residue was dissolved in dichloromethane (10 mL), dried over anhydrous Na_2SO_4, filtered, and finally concentrated to dryness in vacuo to yield the title compound as a yellow amorphous solid. Size and percent yield are yet to be determined. H^1-NMR located in SI section.

*Ethyl 4-iodo-3-(4-methoxy-3-((tetrahydro-2H-pyran-2-yl)oxy)phenyl)-5-(3,4,5-trimethoxyphenyl)-1H-pyrrole-2-carboxylate (**4a**)*

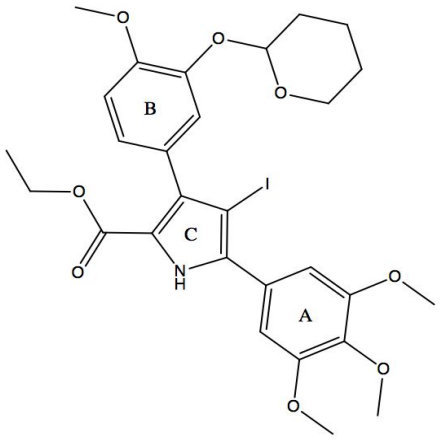

Glycine ethyl ester hydrochloride (0.40 g, 2.86 mmol, 1.22 equiv) was placed in a two-necked round-bottom flask equipped with a reflux condenser, and pyridine (20 mL) was added. The suspension was heated to reflux at 120 °C and a solution of chalcone (3a) (1.00 g, 2.35 mmol, 1.00 equiv) in pyridine (34 mL) was added dropwise to the clear and colorless refluxing solution. Stirring and reflux were maintained for at least 24 h, and then a solution of copper(II) acetate (0.96 g, 2.35 mmol, 1.00 equiv) in pyridine (38.4 mL) was added to the refluxing brown solution. After 4 h, the temperature of the oil bath was decreased to 70 °C and a solution of N-iodosuccinimide (0.72 g, 2.35 mmol, 1.00 equiv) in acetonitrile (39.6 mL) was added. The reaction mixture was kept at 70 °C for an additional 6 h and then concentrated in vacuo. The residual pyridine was removed by azeotropic distillation with toluene (40 mL). Solid was then dissolved in dichloromethane (60 mL) and underwent a liquid-liquid extraction with 0.1 M Na_2EDTA $2H_2O$ (3 x 20 mL) and brine (30 mL), dried with Na_2SO_4, filtered, and concentrated under reduced pressure to collect the remaining brown solid. Further purification was conducted by flash column chromatography (silica gel, cyclohexane/ethyl acetate = 75:25) to afford the title
compound as a light yellow to colorless crystalline solid (1.50 g, 78%) Unconfirmed via spectral data.

*Ethyl 4-iodo-3,5-bis(3,4,5-trimethoxyphenyl)-1H-pyrrole-2-carboxylate (**4b**)*

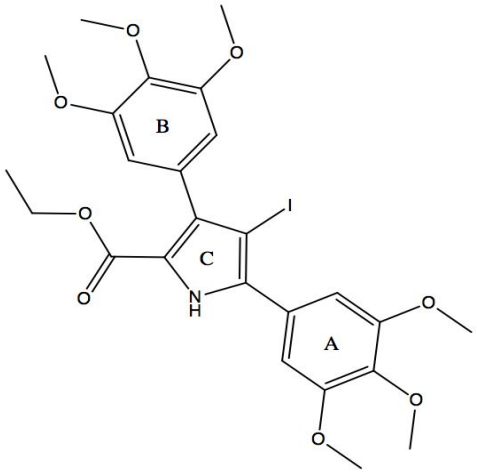

Glycine ethyl ester hydrochloride (0.18 g, 0.8 mmol, 1.25 equiv) was placed in a two-necked round-bottom flask equipped with a reflux condenser, and pyridine (3 mL) was added. The suspension was heated to reflux at 120 °C and a solution of chalcone (3b) (0.25 g, 0.64 mmol, 1.00 equiv) in pyridine (2 mL) was added dropwise to the clear and colorless refluxing solution. Stirring and reflux were maintained for at least 24 h, and then a solution of copper(II) acetate (0.24 g, 1.3 mmol, 2.03 equiv) was added to the refluxing brown solution. After 4 h, the temperature of the oil bath was decreased to 70 °C and a solution of N-iodosuccinimide (0.18 g, 0.8 mmol, 1.25 equiv) in acetonitrile (10 mL) was added. The reaction mixture was kept at 70 °C for an additional 6 h and then concentrated in vacuo. The residual pyridine was removed by azeotropic distillation with toluene (15 mL). Solid was dissolved in dichloromethane (25 mL) and underwent a liquid-liquid extraction with 0.1 M Na_2EDTA $2H_2O$ (3 x 20 mL) and brine (30 mL), dried with Na_2SO_4, filtered, and concentrated under reduced pressure to collect the remaining brown solid. Further purification was conducted by flash column chromatography (silica gel, cyclohexane/ethyl acetate = 30:70) to afford the title compound as a light yellow to colorless crystalline solid (0.28 g, 75%) Unconfirmed via spectral data.

*Ethyl 4-iodo-5-(4-methoxyphenyl)-3-(3,4,5-trimethoxyphenyl)-1H-pyrrole-2-carboxylate (**4c**)*

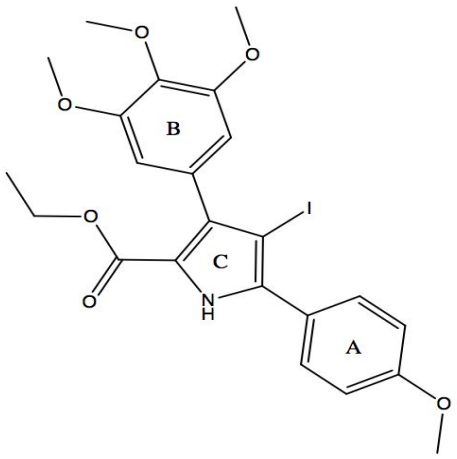

Glycine ethyl ester hydrochloride (0.073 g, 0.53 mmol, 1.15 equiv) was placed in a two-necked round-bottom flask equipped with a reflux condenser, and pyridine (4 mL) was added. The suspension was heated to reflux at 125 °C and a solution of chalcone (3d) (0.14 g, 0.46 mmol, 1.00 equiv) in pyridine (7 mL) was added dropwise to the clear and colorless refluxing solution. Stirring and reflux were maintained for at least 24 h, and then a solution of copper (II) acetate (0.17 g, 0.94 mmol, 2.04 equiv) in pyridine (7 mL) was added to the refluxing brown solution. After 4 h, the temperature of the oil bath was decreased to 70 °C and a solution of N-iodosuccinimide (0.13 g, 0.58 mmol, 1.25

equiv) in acetonitrile (4.5 mL) was added. The reaction mixture was kept at 70 °C for an additional 6 h and then concentrated in vacuo. The residual pyridine was removed by azeotropic distillation with toluene (20 mL). Solid was dissolved in dichloromethane (20 mL) and underwent a liquid-liquid extraction with 0.1 M Na_2EDTA $2H_2O$ (3 x 20 mL) and brine (30 mL), dried with Na_2SO_4, filtered, and concentrated under reduced pressure to collect the remaining brown solid. Further purification was conducted by flash column chromatography (silica gel, cyclohexane/ethyl acetate = 730:70) to afford the title compound as a light yellow to colorless crystalline solid (0.13 g, 67%) Unconfirmed via spectral data.

*Ethyl 3,5-bis(3,4,5-trimethoxyphenyl)-1H-pyrrole-2-carboxylate (**4d**)*

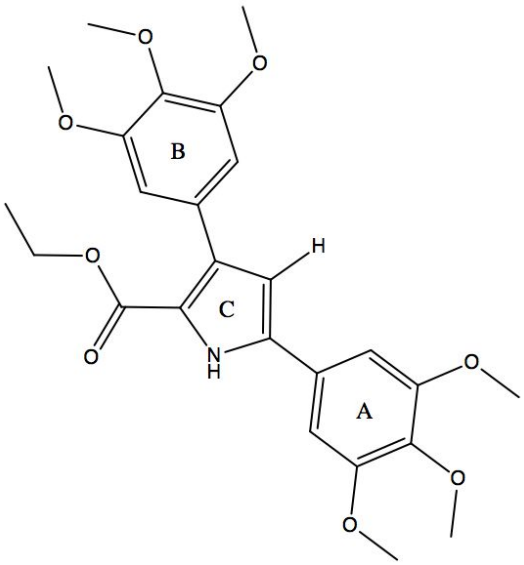

Glycine ethyl ester hydrochloride (0.1886 g, 1.35 mmol, 1.05 equiv) was placed in a two-necked round-bottom flask equipped with a reflux condenser, and pyridine (5 mL) was added. The suspension was heated to reflux at 125 °C and chalcone (3b) (0.50 g, 1.29 mmol, 1.00 equiv) was added to the clear and colorless refluxing solution. Stirring and reflux were maintained for at least 24 h, and then a solution of copper (II) acetate (0.28 g, 1.54 mmol, 1.2 equiv) was added to the refluxing brown solution. After 4 h, the heat was removed. The residual pyridine was removed by azeotropic distillation with toluene (30 mL). Solid was dissolved in dichloromethane (30 mL) and underwent a liquid-liquid extraction with 0.1 M Na_2EDTA $2H_2O$ (3 x 30 mL) and brine (50 mL), dried with Na_2SO_4, filtered, and concentrated under reduced pressure to collect the remaining brown solid. (0.42 g, 70%) Unconfirmed via spectral data.

6. Conclusion

Overall, the objective of this project has transitioned from primarily isolating the final products of both the first and second foci into a methodological investigation to seek the best reaction conditions for a given reaction within the scope of the synthetic schemes. Each chalcone now has its own specific procedure which is followed in order to provide not only high purity, but also high percent yields.

The specific reaction conditions for lamellarin pyrroles and their iodopyrrole intermediates are still under investigation. Similar assessment strategies that were used with chalcones are being applied to these compounds. Hopefully, this will not only provide better procedures and reaction conditions, yet also a better understanding of each of the three steps required to form these intermediates.

The *in-silico* docking performed on the discussed analogs of CA-4 has allowed for various predictions to be made regarding the potential outcomes of (1) their *in-vitro* and potentially *in-vivo* binding affinities to the tubulin-colchicine binding sites and (2) their abilities to induce proapoptotic effects within the cell preventing it from continuing to

proliferate. For example, some of the analogs with the worst binding affinities to the active site (such as the lamellarin pyrrole alkyne **5a**) are expected to have the strongest biological potencies due to their functional groups and interactions. These results have also shown that the hydroxyl groups have more interactions than the methoxy groups and that in the future, changing some of the functional groups on the A-ring to hydroxyls may improve the compound's overall bioactivity and binding affinity.

An *in-vitro* MTT bioassay is in the process of being performed and results are expected to follow the hypotheses formed from the *in-silico* docking results.

Future work regarding the second focus is to computationally dock the distances between the A-D and B-D rings for the lamellarin pyrrole alkynes and determine which way the compound will cyclize thus predicting which rings (A-E or B-E) will become fused together as this depends on the different substituents on both A and B rings.

The results of these projects will provide a better insight into the effects of lamellarin pyrrole analogs in the tubulin-colchicine complex and in mutated DNA environments. By manipulating these novel compounds into serving a variety of functions to both combat multidrug resistant cancer cells and cleave foreign DNA, the field of cancer research will expand and propagate new questions to be answered.

7. Bibliography

1. SEER Stat Fact Sheets: Cancer of Any Site https://seer.cancer.gov/statfacts/html/all.html (accessed Nov 17, 2016).
2. Chaplin, D., Prise, S., Tozer, G., Pettit, G., and Dark, G. (1997) Combretastatin A-4, an agent that displays selective toxicity towards tumour vasculature. *European Journal of Cancer*. Ref.
3. Pettit George R, Cragg Gordon M, Herald Delbert L, Schmidt Jean M, Lohavanijaya Prasert. Isolation and structure of combretastatin. *Can J Chem*. 1982, *60,* 1374–1376.
4. Pettit George R, Singh Sheo Bux, Niven Margaret L, Hamel Ernest, Schmidt Jean M. Isolation, structure, and synthesis of combretastatins A-1 and B-1, potent new inhibitors of tubulin assembly, derived from *Combretum caffrum*. *J Nat Prod.* 1987, *50*, 119–131.
5. Dialer, Clemes; Imbri, Dennis; Hansen, Steven Peter; Opatz, Till. Synthesis of Lamellarin D Trimethyl Ether and Lamellarin H via 6π-Electrocyclization. *J. Org. Chem.* 2015. *80*, 22, 11605–11610.
6. Rustin, G. J.; Shreeves, G.; Nathan, P. D.; Gaya, A.; Ganesan, T, S.; Wang, D; Boxall, J.; Poupard, L.; Chaplin, D. J.; Stratford, M. R. L; Balkissoon, J.; Zweifel, M; *Br J. Cancer.* 2010. 102, 1355-1360.
7. Dark GG, et al. Cancer Res 1997, 57(10), 1829-1834.
8. Fosbretabulin (Combretastatin A4 Phosphate (CA4P)) Disodium. Fosbretabulin (Combretastatin A4 Phosphate (CA4P)) Disodium | Microtubule Associated inhibitor | Read Reviews & Product Use Citations.
9. Combretastatin A4. Combretastatin A4 | Microtubule Associated inhibitor | Read Reviews & Product Use Citations.
10. Nielsen, Thomas; Bentzen, Lise; Pedersen, Michael; Tramm, Trine; Rijken, Paul F.; Bussink, Jordan; Horsman, Michael R.; and Ostergaard, Leif. CA-4 Phosphate Affects Tumor Vessel Volume and Size Distribution as Assessed Using MRI-Based Vessel Size Imaging. *Clin Cancer Res.* 2012. 18, 6469-6477.
11. Reddy, MV; Ridley, CP; Bushman FD; Faulkner DJ. Total Synthesis and Evaluation of Lamellarin-alpha 20-Sulfate analogues. 2002. *10*, 3285-3290.
12. Ohta, Takeshi; Fukuda, Tsutomu; Ishibashi, Fumito; Iwao, Masatomo. Design and Synthesis of Lamellarin D Analogues Targeting Topoisomerase I. *J. Org. Chem.* 2009, *74*, 8143–8153.
13. Gouverneur, Véronique. Fluorine in Pharmaceutical and Medicinal Chemistry: From Biophysical Aspects to Clinical Applications. 2012. *6*, 1-15.
14. Gouverneur, Véronique; Purser, Sophie; Moore, Peter R.; Swallow, Steve. Fluorine in Medicinal Chemistry. 2008. 2,
15. Vallabhajosula, Shankar; Imaging in Neurodegenerative Disorders. 2015. 1, 140-161.
16. Gaspari, Roberto; Rozas, Isabel; Prote, Andrea E.; Bargsten, Katja; Cavalli, Andrea; Steinmetz, Michel O. Understanding the binding of *cis* and *trans* Isomers of Combretastatin to Tubulin. *Chem*. 2017. 2, 15-17.
17. Reddy, M. V. R., Rao, M. R., Rhodes, D., Hansen, M. S. T., Rubins, K., Bushman, F. D., Venkateswarlu, Y., and Faulkner, D. J. Lamellarin α 20-Sulfate, an Inhibitor of HIV-1 Integrase Active against HIV-1 Virus in Cell Culture. *J. Med. Chem*. 1999. 42, 1901–1907.

18. Ridley, C. Total synthesis and evaluation of lamellarin α 20-Sulfate analogues. *Bioorg. Med. Chem.* 2002. 10, 3285–3290.
19. Bailly, Christian. "Anticancer Properties of Lamellarins." *MDPI*. Multidisciplinary Digital Publishing Institute, 19 Feb. 2015. Web. 10 May 2017.
20. Jean, Mikael; Tomasi, Sophie; Van De Weghe, Pierre. When the nine-membered enediynes play hide and seek. *Org. Biomol. Chem.* 2012. 10, 7453.
21. Ishida, N.; Miyazaki, K.; Kumagai, K.; Rikimaru, M. *J. Antibiot.* 18 (1965) 68
22. Avendaño, Carmen; Menéndez, J. Carlos. Anticancer Drugs Targeting Tubulin and Microtubules. 2008. 229-249.